ChemPubSoc Europe

DOI: 10.1002/cmdc.201600055

CHEMMEDCHEM Full Papers

Design, Synthesis, and Evaluation of Acrylamide Derivatives as Direct NLRP3 Inflammasome Inhibitors

Mattia Cocco,[a] Gianluca Miglio,[a] Marta Giorgis,[a] Davide Garella,[a] Elisabetta Marini,[a] Annalisa Costale,[a] Luca Regazzoni,[b] Giulio Vistoli,[b] Marica Orioli,[b] Raïhane Massulaha-Ahmed,[c] Isabelle Détraz-Durieux,[c] Marine Groslambert,[c] Bénédicte F. Py,[c] and Massimo Bertinaria*[a]

NLRP3 inflammasome plays a key role in the intracellular activation of caspase-1, processing of pro-inflammatory interleukin-1β (IL-1β), and pyroptotic cell death cascade. The overactivation of NLRP3 is implicated in the pathogenesis of autoinflammatory diseases, known as cryopyrin-associated periodic syndromes (CAPS), and in the progression of several diseases, such as atherosclerosis, type-2 diabetes, gout, and Alzheimer's disease. In this study, the synthesis of acrylamide derivatives and their pharmaco-toxicological evaluation as potential inhibitors of NLRP3-dependent events was undertaken. Five hits were identified and evaluated for their efficiency in inhibiting IL-1β release from different macrophage subtypes, including CAPS mutant macrophages. The most attractive hits were tested for their ability to inhibit NLRP3 ATPase activity on human recombinant NLRP3. This screening allowed the identification of **14**, 2-(2-chlorobenzyl)-*N*-(4-sulfamoylphenethyl)acrylamide, which was able to concentration-dependently inhibit NLRP3 ATPase with an IC_{50} value of 74 μM. The putative binding pose of **14** in the ATPase domain of NLRP3 was also proposed.

Introduction

Inflammation is a key physiological response to harmful stimuli, including exogenous pathogens and endogenous danger signals. Cells of the innate immune system recognize pathogen-associated molecular patterns (PAMPs) and danger-associated molecular patterns (DAMPs) through germline-encoded pattern recognition receptors, such as Toll-like receptors (TLRs) and nucleotide oligomerization domain (NOD)-like receptors (NLRs).[1,2] A vast array of PAMPs and DAMPs has been recognized so far, including microbial products (e.g., lipopolysaccharide; LPS), molecules released after cell lysis (e.g., adenosine triphosphate; ATP),[3,4] hypotonic stress,[5,6] and particles produced as a consequence of an altered metabolism, such as cholesterol crystals,[7] sodium monourate crystals,[8] and β-amyloid aggregates.[9] Despite the well-established protective role, uncontrolled and/or protracted inflammation is thought to exert detrimental effects, by both exacerbating underlying pathological processes and promoting the onset of new disorders.

In the last decades, several studies have highlighted the pivotal role of inflammasomes, which are large intracellular protein complexes, in the molecular control of inflammatory processes.[10–12] In particular, the NLR family pyrin-domain-containing 3 (NLRP3) inflammasome is the best characterized and the most widely implicated pattern recognition receptor in caspase-1-dependent pro-inflammatory events, including both interleukin (IL)-1β maturation and cell death by pyroptosis. The pathological role of NLRP3 inflammasome activation has been better established in a subset of genetic disorders known as cryopyrin-associated periodic syndromes (CAPS), also known as cryopyrinopathies. CAPS are characterized by recurrent episodes of severe systemic inflammation and are related to the presence of gain-of-function mutations in the NLRP3 gene.[13–15] NLRP3 and oligomeric ASC particles have also been detected in the serum of patients with active CAPS, in which they mediate the amplification of the inflammatory response.[16] Moreover, compelling data have implicated inflammasome activation in the progression of several noncommunicable diseases, such as atherosclerosis,[7] type-2 diabetes mellitus,[17] gout,[8] and Alzheimer's disease.[18]

This evidence has increased the interest in the discovery of agents able to prevent inflammasome activation, which is regarded as a promising therapeutic strategy to decrease chronic inflammation and associated damage in different pathological settings. To date, different approaches have been pursued,[19] among which reversible or irreversible modification of reactive cysteine (Cys) residues of relevant proteins seems to be the

[a] M. Cocco, Dr. G. Miglio, Dr. M. Giorgis, Dr. D. Garella, Dr. E. Marini, A. Costale, Prof. M. Bertinaria
Dipartimento di Scienza e Tecnologia del Farmaco, Università degli Studi di Torino, Via P. Giuria 9, 10125 Torino (Italy)
E-mail: massimo.bertinaria@unito.it

[b] Dr. L. Regazzoni, Prof. G. Vistoli, Prof. M. Orioli
Dipartimento di Scienze Farmaceutiche, Università degli Studi di Milano, Via Mangiagalli 25, 20133 Milano (Italy)

[c] R. Massulaha-Ahmed, I. Détraz-Durieux, M. Groslambert, Dr. B. F. Py
CIRI, International Center for Infectiology Research, Inserm U1111, CNRS UMR 5308, Ecole Normale Supérieure de Lyon, Université Lyon 1, 21 avenue Tony Garnier, 69007 Lyon (France)

Supporting Information and the ORCID identification number(s) for the author(s) of this article can be found under http://dx.doi.org/10.1002/cmdc.201600055.

prevalent one. Structure-based drug design would help in the development of safer covalent drugs targeting suitably positioned Cys residues. However, structural knowledge of NLRP3 still needs to be fully understood: apart from the disulfide bridge between Cys8 and Cys108 in the NLRP3 pyrin domain, little is known of the other 43 Cys residues of NLRP3 (UniProt ID: Q96P20-1).

The crystal structure of the NLRP3 ATPase active site is not yet available; nonetheless, this pocket in the NACHT domain could be an interesting target to develop NLRP3 inhibitors.[20] In fact, ATP hydrolysis is required to have active NLRP3 in the cytosol.[21]

In a previous study, our group developed a series of electrophilic warheads preventing the NLRP3-dependent and ATP-triggered cell death of differentiated and primed THP-1 cells, which is a cellular model of macrophage pyroptosis.[22] This proof of concept study demonstrated that molecules endowed with the ability to behave as Michael acceptors could efficiently prevent pyroptotic cell death by inhibiting NLRP3 signaling. A complex mechanism involving multitarget action owing to the reactivity of the electrophile could explain this effect.

The most promising warheads identified (Figure 1, compounds **1**–**3**) also proved able to directly inhibit the NLRP3

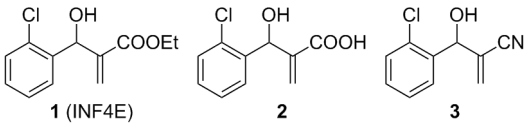

Figure 1. Electrophilic warheads that prevent NLRP3-dependent pyroptosis and that inhibit NLRP3 ATPase activity.

ATPase activity of isolated enzyme. Unfortunately, compounds **1** and **3** exerted a certain degree of cytotoxicity,[22] which could be related to their high reactivity. With the aim of limiting this issue, in this work we developed a series of acrylamide derivatives. The use of the acrylamide functionality should enable the development of safer compounds by tuning down the reactivity of the electrophilic warhead. The acrylamide functionality has already been exploited in the generation of approved covalent drugs such as EGFR and BTK inhibitors, among others (Figure 2).[23]

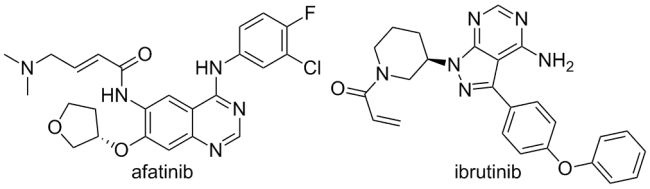

Figure 2. Structures of approved acrylamide-based kinase inhibitors.

The molecules depicted in Figure 3 were designed by modulation of general structure **I**. In this series of compounds, we maintained the *o*-chloro-substituted benzene ring, as it was previously identified as the optimal aromatic portion in acrylate-based inhibitors[22] in the western part of the molecules. To investigate the role of the hydroxy group in the reactivity and/or the cytotoxicity of this class of electrophilic compounds, a small set of N-substituted compounds bearing a hydroxy group in the benzylic position (i.e., compounds **4**–**7**) was synthesized and compared with a series of close analogues deprived of the hydroxy group (i.e., compounds **8**, **9**, **11**). Removal of the OH group was then coupled to different N-substitution patterns (i.e., compounds **10**, **12**–**16**) to explore the possibility of increasing the activity through direct NLRP3 inhibition.

In particular, compounds **14** (INF58) and **15** were designed by using a ligand-merging strategy. Both **14** and **15** share the Michael-acceptor moiety present in compound **1** (INF4E) and a sulfonamide or a sulfonylurea portion typical of compound 16673-34-0[24] and glyburide,[25] two known NLRP3-network inhibitors (Figure 4). Finally, the molecular pharmacophore dimerization strategy was considered in the design of compound **16** (Figure 3).

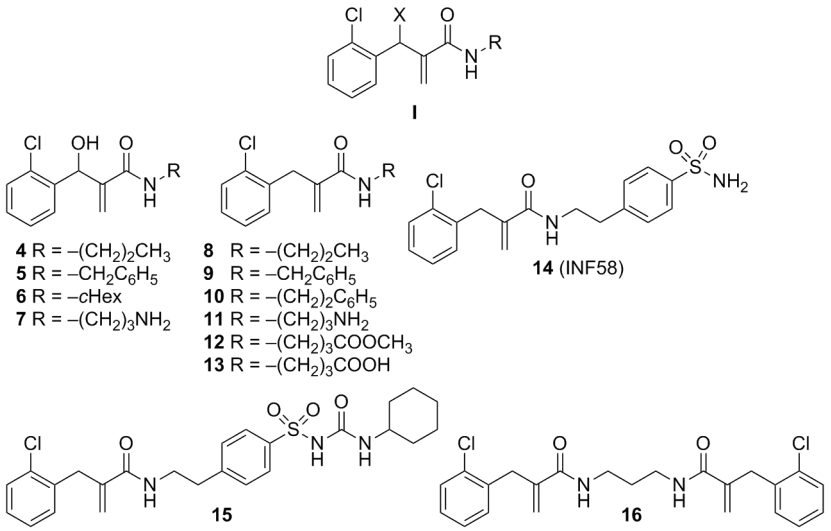

Figure 3. General structure **I** and structures of designed compounds **4**–**16**.

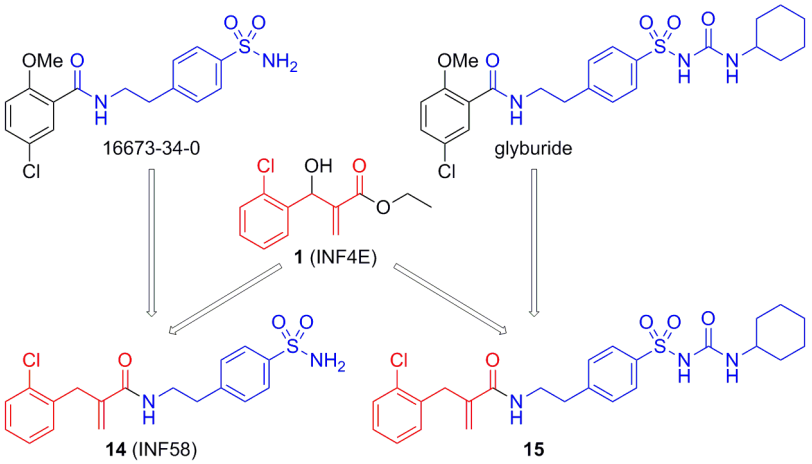

Figure 4. Ligand merging design of compounds **14** (INF58) and **15**.

Results and Discussion

Chemistry

Synthesis

To synthesize acrylamides **4**–**7** bearing a hydroxy group in the benzylic position, we first followed the route previously described for the synthesis of compound **4** by employing the 2-(1*H*-benzotriazol-1-yl)-1,1,3,3-tetramethyluronium hexafluorophosphate (HBTU)/hydroxybenzotriazole (HOBt)-mediated coupling of 2-[(2-chlorophenyl)(hydroxy)methyl]acrylic acid (**2**, Figure 1) with *n*-propylamine.[22] However, the use of this route with other primary amines gave rise to a complex mixture of products with no possibility to obtain the desired compounds with purities >95% by chromatography. This may have been due to the presence of the highly reactive OH group in compound **2**. To overcome this inconvenience, we followed a different route (Scheme 1). The hydroxy group in compound **1** was protected by using *tert*-butyldimethylsilyl chloride (TBDMSCl), and obtained intermediate **17** was subsequently hydrolyzed with LiOH in a CH_3CN/H_2O mixture to afford **18** in 70% yield from **1**. Obtained acid **18** was coupled with the appropriate amine by using dicyclohexylcarbodiimide (DCC) and *N*-hydroxysuccinimide (NHS) to afford derivatives **19a**–**d**. Derivatives **19a**–**c** were deprotected by using tetrabutylammonium fluoride (TBAF) in THF to give desired compounds **4**–**6** in good overall yields (41–49%). Compound **19d** was treated with CF_3CO_2H to remove both the TBDMS and *tert*-butoxycarbonyl (Boc) protecting groups to afford desired acrylamide **7**.

Acrylamides **8**–**14**, lacking the hydroxy group at the benzylic position, were synthesized by using the route depicted in Scheme 2. Commercially available 2-chlorobenzyl bromide was treated with ethyl (diethoxyphosphoryl)acetate to afford phosphonate **20**, which underwent Horner–Wadsworth–Emmons reaction with paraformaldehyde to afford compound **21**. Acrylic ester **21** was hydrolyzed with NaOH to obtain acid **22**, which was then converted into activated ester by **23** using DCC and NHS. *N*-Hydroxysuccinimidyl ester **23** was purified by flash chromatography and was then treated with selected amines to obtain derivatives **8**–**10**, **12**–**14** in overall yields of 20–32%.

To obtain final compound **11**, a deprotection step with the use of 10% CF_3CO_2H in CH_2Cl_2 was required. Sulfonylurea derivative **15** was synthesized by treating sulfonamide **14** with cyclohexyl isocyanate in basic medium. Finally, derivative **16** bearing two electrophilic moieties was obtained by direct coupling of **11** with a stoichiometric amount of **23** and an excess amount of diisopropylethylamine (DIPEA) (Scheme 2).

Reactivity as Michael acceptor

The acrylamide functionality has been used in the development of covalent kinase inhibitors.[26] Covalent inhibitors can possess advantages over their reversible counterparts, such as increased biochemical efficiency, longer duration of action, the

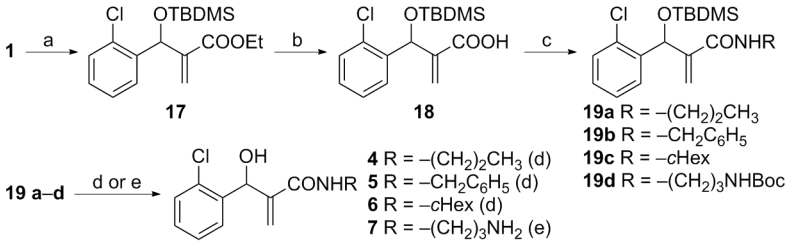

Scheme 1. *Reagents and conditions*: a) TBDMSCl (1.5 equiv), imidazole (2.5 equiv), DMF, RT, 16 h; b) LiOH (10 equiv), CH_3CN/H_2O 1:1, 60 °C, 16 h; c) 1. DCC (1 equiv), NHS (1 equiv), DIPEA (1.5 equiv), THF, 0 °C, 15 min, RT, 2 h, 2. amine (2 equiv), RT, 16 h; d) TBAF (1.1 equiv), THF, RT, 1 h; e) CF_3CO_2H, CH_2Cl_2, RT, 2 h.

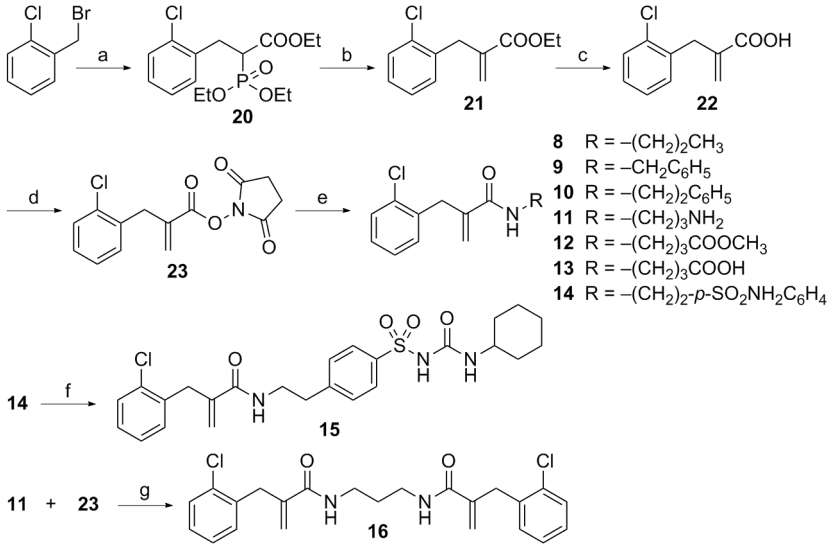

Scheme 2. *Reagents and conditions*: a) ethyl (diethoxyphosphoryl)acetate (1.2 equiv), NaH (1.4 equiv), DMF, 0 °C, 1 h, RT, 18 h; b) paraformaldehyde (6.5 equiv), K_2CO_3 (3 equiv), H_2O, 90 °C, 16 h; c) NaOH, EtOH, RT, 16 h; d) DCC (1 equiv), NHS (1 equiv), THF, 0 °C, 16 h; e) for compounds **8**–**10**, **12**–**14**: H_2NR (1.5 equiv), CH_2Cl_2/DMF 2:1, Et_3N (2 equiv), RT, 2–16 h; for compound **11**: 1. H_2NR (1.5 equiv), CH_2Cl_2/DMF 2:1, Et_3N (2 equiv), RT, 3 h, 2. CF_3CO_2H (10%), CH_2Cl_2, RT, 1 h; f) cyclohexyl isocyanate (1.6 equiv), K_2CO_3 (3 equiv), dry acetone, reflux, 16 h; g) DIPEA (1.2 equiv), DMF, RT, 1 h.

potential to avoid drug-resistance mechanisms, and the potential for improved efficacy, which could be reflected in lower therapeutic doses.[23]

However, covalent protein modification has also been implicated in immunotoxicity and idiosyncratic reactions. This kind of toxicity is particularly evident if the covalent inhibitor is highly reactive and/or lacks specificity.[27,28] To rationally design electrophiles for covalent inhibition it is useful to tune both their intrinsic reactivity and their noncovalent protein–inhibitor interactions to optimize selectivity against the desired target(s).

Accordingly, the electrophilic reactivities of synthesized compounds **4**–**16** and reference compound **1** were checked by using the kinetic cysteamine chemoassay previously described.[22] Compounds were mixed with an equimolar amount of cysteamine (CAM) in pH 7.4 phosphate-buffered solution at 37 °C by using CH_3CN (12.5%) as the co-solvent. The progress of the reaction was monitored by adding 5,5′-dithio-bis(2-nitrobenzoic acid) (DTNB) at different time points over a period of 90 min. None of the tested acrylamides proved reactive under the conditions used. Reference compound **1** showed a second-order rate constant (k_2) value of $0.824 \pm 0.017\ M^{-1}s^{-1}$ with acetonitrile as the co-solvent ($k_2 = 0.866 \pm 0.006\ M^{-1}s^{-1}$ with 2.5% DMSO as the co-solvent),[22] whereas compound **4**, which was previously found to react slowly with CAM in DMSO ($k_2 = 0.126 \pm 0.005\ M^{-1}s^{-1}$),[22] was unreactive with less-polar acetonitrile. These data indicated that the reactivity of this series of electrophilic compounds was efficiently tuned down by employing the acrylamide functionality.

To demonstrate the ability of these acrylamides to behave as Michael acceptors, model compound **14** was treated with 10 molar equivalents of CAM in pH 7.4 phosphate-buffered solution at 37 °C by using CH_3CN as the co-solvent. The decrease in the concentration of compound **14** was monitored by ultra-high-performance liquid chromatography (UHPLC) for 7 h. Consumption of the electrophile was detected and plotted as the natural log to check for linearity and pseudo-first-order reaction kinetics, $k_{pseudo1st}$.[29] Under these conditions, compound **14** was indeed able to react slowly with CAM, with a $k_{pseudo1st}$ value of $0.627 \pm 0.013\ min^{-1} \times 10^{-3}$ (Figure S1, Supporting Information).

Finally, to evaluate the potential of this class of compounds to trigger idiosyncratic hypersensitivity reactions, all the compounds were checked for their ability to bind human serum albumin. Compounds were added into fresh human serum at a 1 mM concentration ($CH_3CN < 10\%$ *v/v*) and were incubated for 3 h at 37 °C. Serum aliquots were diluted 200-fold into H_2O/CH_3CN/HCO_2H (70/30/0.1 *v/v/v*), centrifuged, and analyzed by ESI-MS as previously reported.[30] None of the acrylamide derivatives was able to covalently react with albumin. On the contrary, compound **1** produced a modification of $65 \pm 5\%$ of albumin by generation of three covalent adducts. Collectively, these data showed that the reactivity of this class of compounds was decreased to a level that should not promote adverse idiosyncratic reactions mediated by unspecific binding to human serum albumin.

Pharmacology

Antipyroptotic activity and cytotoxicity

The synthesized compounds were initially evaluated for their ability to prevent the NLRP3-dependent pyroptosis of phorbol myristate acetate (PMA)-differentiated THP-1 cells. In this model, the NLRP3 inflammasome-dependent events follow a two-stage process. In the first stage (i.e., priming), NLRP3 ex-

pression is induced through NF-κB-mediated signaling. In the second stage (i.e., activation), NLRP3 inflammasome is assembled and activated following cell exposure to different stimuli. In our experiments, THP-1 cells were primed with LPS and activated with ATP, as previously described.[22] Cell death was quantified by measuring lactate dehydrogenase (LDH) activity in the cell supernatants. First, to perform a preliminary comparative evaluation, cells were exposed (1 h before the ATP pulse) to the synthesized compounds (i.e., **4**–**16**; all at 10 μM). The antipyroptotic effects were determined and expressed as a decrease in pyroptosis relative to vehicle-alone-treated cells (Table 1). Moreover, as structurally related compounds were demonstrated to exert significant cytotoxicity,[22] the effects of increasing concentrations of the newly synthesized derivatives on the viability of THP-1 cells were evaluated (Table 1).

The ATP-triggered cell death of THP-1 cells (48.0 ± 6.8%) pyroptosis vs. untreated cells was prevented by both compound **1** (positive control; 80.9 ± 5.2%) and the new acrylamide derivatives; their effects ranged from 7.5 ± 5.6% to 69.8 ± 2.6%. Compounds **4**, **5**, and **7**, bearing a hydroxy group in the X position (structure **I**), exerted higher antipyroptotic effects than corresponding analogues **8**, **9**, and **11** lacking the hydroxy group (see **4** vs. **8**, **5** vs. **9**, and **7** vs. **11** in Table 1). Higher intrinsic reactivity, although not measureable with the employed assay, might be responsible for the enhanced antipyroptotic effect of the oxygenated series of compounds. In agreement with this hypothesis, the reactivity of α-methyl-*N*-arylacrylamides was recently shown to increase by introducing a hydroxy group at the α-carbon atom.[29] Notably, a marked decrease in cell viability was measured for THP-1 cells that were cultured in the presence of α-hydroxyalkyl-substituted acrylamides **4**–**6** the concentration required to decrease cell viability by 50% (TC_{50}) was in the range from 43.4 ± 5.2 to 83.5 ± 2.2 μM], whereas higher TC_{50} values (> 100 μM) were generally determined for compounds lacking the OH group in the X position (Table 1). These results indicated that removing the OH group in the α position decreased the cytotoxicity of these acrylamide derivatives. Consequently, further development of OH-substituted compounds was discontinued, and chemical modulation of the *N* substituent was performed by using compound **9** (antipyroptotic effect = 28.0 ± 6.6%; TC_{50} > 100 μM) as the preferred scaffold. In addition, compound **8**, lacking significant antipyroptotic activity, was also considered as a model to gain more complete insight into the activity of this class of compounds.

To evaluate whether the higher activity of **9** relative to that of **8** could be attributed to increased lipophilicity (c log *P* = 3.78 and 3.06, respectively), *N*-phenylethyl derivative **10** (c log *P* = 4.10) was synthesized. Relative to that shown by compound **9**, this derivative exerted larger antipyroptotic effects (49.6 ± 5.7%), which thus confirmed the hypothesis that the relative antipyroptotic activity of these related compounds could depend on their lipophilicity. In addition, upon substituting the *N*-propyl chain in **8** with an amino group at the terminal position, less lipophilic, still poorly active, and more cytotoxic compound **11** was obtained (c log *P* = 1.94; anti-pyroptotic effect = 15.7 ± 0.7%; TC_{50} = 46.5 ± 5.5 μM). The activity was slightly increased upon introducing a methoxycarbonyl (see compound **12**) or a carboxy group (see compound **13**) in the same position (Table 1). Of note, relative to compound **8**, derivatives **11**–**13** are more hydrophilic (c log *P* = 1.94–2.77), which thus indicates that factors other than lipophilicity alone are likely responsible for the pharmaco-toxicological activity of these derivatives. Consistently, compound **16**, formally obtained by dimerization of **8**, exerted only modest antipyroptotic effects (25.2 ± 8.1%), in spite of a high degree of lipophilicity (c log *P* = 4.75). Finally, to obtain more insight into the structure–activity relationship of the acrylamide moiety, the effects exerted by compounds **14** and **15** were studied. Interestingly, 16673-34-0-derived compound **14** exerted effects (45.8 ± 2.9% pyroptosis inhibition) similar to those of **10** despite the decreased lipophilicity (c log *P* = 2.27), whereas highly lipophilic glyburide-derived compound **15** (c log *P* = 4.40) exerted only modest antipyroptotic effects in our model (17.3 ± 2.8%) pyroptosis inhibition.

To better characterize the antipyroptotic activity of these acrylamides, the concentration–response curve of representative derivatives **8**–**10**, **12**, and **14** was studied (Figure 5). The ATP-triggered pyroptosis of THP-1 cells was prevented by these compounds in a concentration-dependent manner: the IC_{50} values ranged from 12.7 to 53.1 μM. Collectively, these data demonstrate that weak electrophiles, obtained by chemical modulation of structure **I** (X = H), can be efficiently used to design and develop nontoxic NLRP3 inhibitors acting as antipyroptotic agents.

Table 1. Inhibitory effect of INF4E (**1**) and compounds **4**–**16** on pyroptotic death of THP-1 cells and cytotoxicity (TC_{50}) in THP-1 cells.

Compd	Pyroptosis decrease [%][a]	TC_{50} [μM][b]	c log *P*[c]
1 (INF4E)	80.9 ± 5.2	67.0 ± 3.4	2.59
4	31.2 ± 6.8	83.5 ± 2.2	2.09
5	69.8 ± 2.6	44.5 ± 1.2	2.75
6	45.9 ± 5.2	43.4 ± 5.2	3.07
7	35.8 ± 5.3	> 100	0.97[d]
8	7.5 ± 5.6	> 100	3.06
9	28.0 ± 6.6	> 100	3.78
10	49.6 ± 5.7	> 100	4.10
11	15.7 ± 0.7	46.5 ± 5.5	1.94[d]
12	34.7 ± 3.5	> 100	2.77
13	38.5 ± 10.8	> 100	2.31[d]
14 (INF58)	45.8 ± 2.9	> 100	2.27
15	17.3 ± 2.8	> 100	4.40
16	25.2 ± 8.1	> 100	4.75

[a] Determined by measuring LDH release in PMA-differentiated and LPS-primed (5 μg mL^{-1}; 4 h) THP-1 cells. Compounds were administered at 10 μM. After 1 h, pyroptosis was triggered with ATP (5 mM). LDH activity was measured 1 h after ATP challenge. Data are the percentage of pyroptosis decrease versus vehicle alone and are the mean ± SEM of three independent experiments. [b] THP-1 cells were exposed to increasing concentrations (0.1–100 μM) of each compound, and cell viability was measured at 72 h by MTT assay; TC_{50} is the molar concentration of compound required to decrease cell viability by 50%; data are the mean ± SEM of three independent experiments. [c] c log *P* was calculated by using ChemBioDraw Ultra 12.0 (CambridgeSoft). [d] c log *P* was calculated for the neutral form.

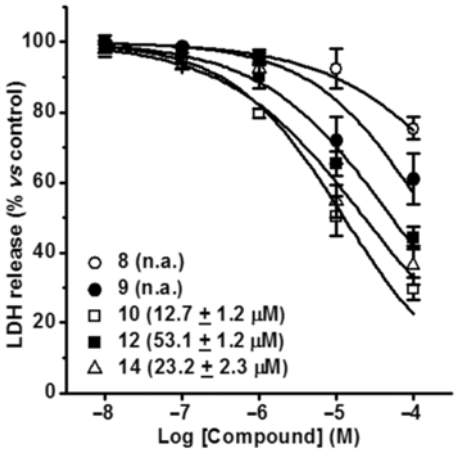

Figure 5. Concentration–response curves of the antipyroptotic effects of compounds **8**, **9**, **10**, **12**, and **14**; IC_{50} values (mean ± SEM of three independent experiments) are reported in brackets; n.a.: not applicable.

Inhibition of IL-1β release from macrophages

We next verified the ability of the most interesting compounds to inhibit NLRP3-dependent IL-1β secretion in macrophages. Murine-immortalized bone-marrow-derived macrophages (BMDMs), primary BMDMs, and primary inflammatory peritoneal macrophages were primed with LPS and then treated with extracellular ATP to activate NLRP3 (Figure 6). Compounds **5**, **10**, **12**, **14**, and **16** were added to the macrophages either simultaneously to LPS treatment or 15 min prior to ATP pulse. All tested compounds significantly inhibited IL-1β secretion if added simultaneously with LPS regardless of the type of macrophage (Figure 6). Most compounds were also effective if added 15 min only before ATP treatment, which suggests that these compounds block NLRP3 activation in the ATP-driven second step and not LPS-dependent priming. Consistently, none of the compounds affected TLR4-dependent NLRP3-independent tumor necrosis factor (TNF)-α release, which demonstrates that they do not target activation of inflammatory genes transcription triggered by LPS.

Inhibition of IL-1β release from CAPS mutant macrophages

Gain-of-function mutations in the NLRP3 gene cause hereditary autoinflammation events referred to as CAPS that correspond to a disease spectrum of three clinically defined disorders: familial cold autoinflammatory syndrome (FCAS), Muckle–Wells syndrome (MWS), and neonatal-onset multisystem inflammatory disease (NOMID). To evaluate the potential of these compounds in CAPS treatment, we tested their ability to dampen the activity of CAPS-associated NLRP3 mutants. We reconstituted mouse immortalized NLRP3 KO BMDMs with murine NLRP3 R258W and A350V (corresponding to the human R260W and A352V mutations, respectively, both associated with MWS) and NLRP3 L351P (corresponding to the human L353P mutation associated with FCAS).[31–33] As previously described,[34,35] LPS priming is sufficient to trigger IL-1β secretion from macrophages expressing NLRP3 R258W, A350V, and L351P.

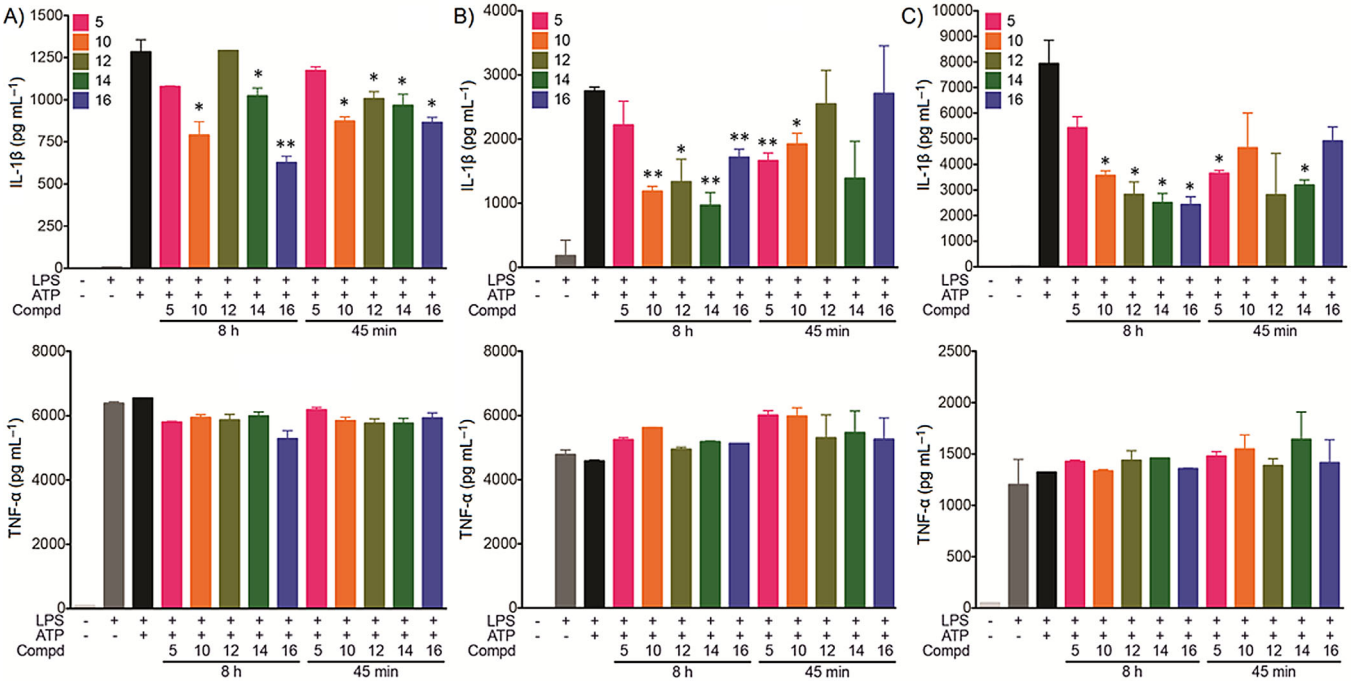

Figure 6. Effects of compounds **5**, **10**, **12**, **14**, and **16** on IL-1β and TNF-α release in A) murine immortalized macrophages, B) bone-marrow-derived macrophages, and C) primary peritoneal macrophages. Macrophages were treated with LPS (50 ng mL^{-1}, 8 h) and ATP (2 mM, 30 min). Compounds (20 μM) were added simultaneously with LPS (8 h) or 15 min before ATP treatment (45 min total). Secretion of IL-1β (top row) and TNF-α (bottom row) in culture supernatants were measured by ELISA. *$p < 0.05$, **$p < 0.01$ versus LPS- and ATP-treated cells; *t*-test. Values are the mean ± SD; results are representative of two independent experiments, each performed in duplicate.

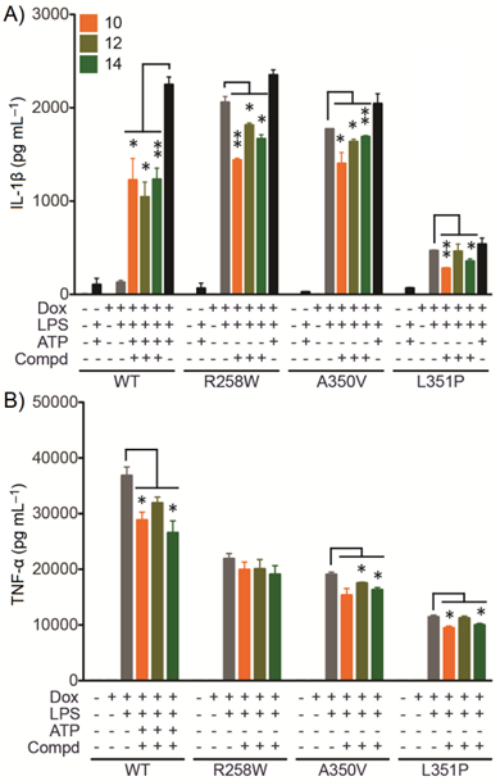

Figure 7. Effects of compounds **10**, **12**, and **14** on A) IL-1β and B) TNF-α released by BMDMs expressing NLRP3 WT, R258W, A350V, or L351P mutants. Immortalized murine NLRP3 KO BMDMs reconstituted with wild-type or mutant NLRP3 were treated with doxycycline (0.1 μg mL^{-1}, 24 h), LPS (50 ng mL^{-1}, 8 h), and ATP (2 mM, 30 min). Compounds (20 μM) were added simultaneously with LPS (8 h). Secretion of IL-1β and TNF-α in culture supernatants were measured by ELISA. *$p < 0.05$, **$p < 0.01$ versus LPS-treated cells in mutant BMDMs; *$p < 0.05$, **$p < 0.01$ versus LPS and ATP in wild-type BMDMs; *t*-test. Values are the mean ± SD; results are representative of two independent experiments, each performed in duplicate.

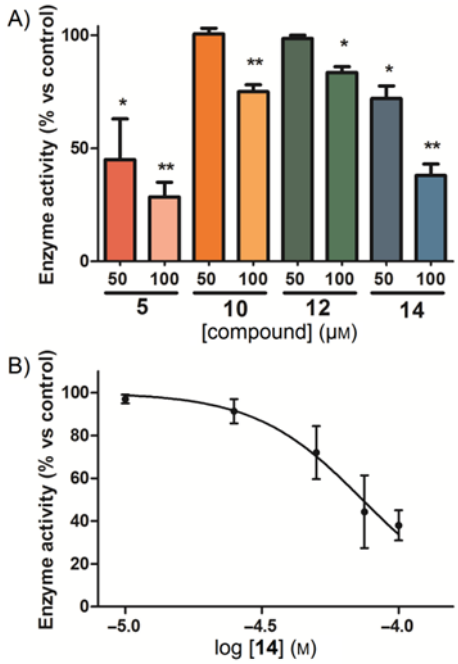

Figure 8. A) Inhibition of NLRP3 ATPase activity of selected compounds **5**, **10**, **12**, and **14**; values are the mean ± SEM of three independent experiments. *$p < 0.05$, **$p < 0.01$ versus vehicle-treated enzyme; *t*-test. B) Concentration–response curve for derivative **14** (INF58).

Compounds **10**, **12**, and **14** selected for this kind of experiment inhibited ATP-dependent IL-1β secretion in LPS-primed macrophages expressing wild-type (WT) NLRP3 (Figure 7). Compound **10** inhibited LPS-induced IL-1β secretion by macrophages expressing NLRP3 R258W, A350V, and L351P. Compound **14** inhibited LPS-induced IL-1β secretion by macrophages expressing NLRP3 R258W and L351P, whereas the effect of compound **12** was restricted to macrophages expressing R258W.

Inhibition of NLRP3 ATPase activity

The ability of compounds **5**, **10**, **12**, and **14** to inhibit the NLRP3 ATPase activity was tested on purified human recombinant enzyme. Human recombinant NLRP3 was incubated at 37 °C in the presence of different concentrations (50 and 100 μM) of tested compounds for 15 min. ATP was then added, and the mixture was incubated at 37 °C for another 40 min. The amount of ATP converted into adenosine diphosphate (ADP) was determined by luminescence by using the ADP-Glo assay. The obtained results, expressed as percentage of residual enzyme activity with respect to vehicle-treated enzyme, are reported in Figure 8A. All the compounds inhibited NLRP3 ATPase activity upon testing at 100 μM, whereas only derivatives **5** and **14** inhibited the enzyme at 50 μM. We next verified the ability of compound **14**, able to prevent pyroptotic cell death and to inhibit IL-1β release from different macrophage lines and devoid of significant toxicity, to concentration-dependently inhibit ATPase activity of NLRP3 protein (Figure 8B). The enzymatic activity was indeed decreased in a concentration-dependent manner with a calculated IC_{50} of 74 μM (95% confidence interval: 63–86 μM), which demonstrated that NLRP3 was a direct target of compound **14** (INF58).

Computational studies

As discussed above, compound **14** and other analogues from this class of acrylamide derivatives proved able to inhibit NLRP3 ATPase activity. We then applied a computational approach to predict the putative binding mode of **14** and other synthesized compounds in the ATP binding pocket in the NACHT domain of NLRP3. As explained in the *Computational methods* subsection of the Experimental Section below and as depicted in Figure 9 (in orange), preliminary docking analysis involved the natural ligand ATP with the view to assess the reliability of the modeled binding pocket further. Satisfactorily, the computed complex is in line with the reported data,[36] as the phosphate groups are seen to stabilize ion pairs with Lys232 and Arg237 plus H-bonds with Thr233 and His522. The Arg237 residue also contacts the ATP adenine base, the 6-amino group of which elicits a reinforced H-bond with Lys238.

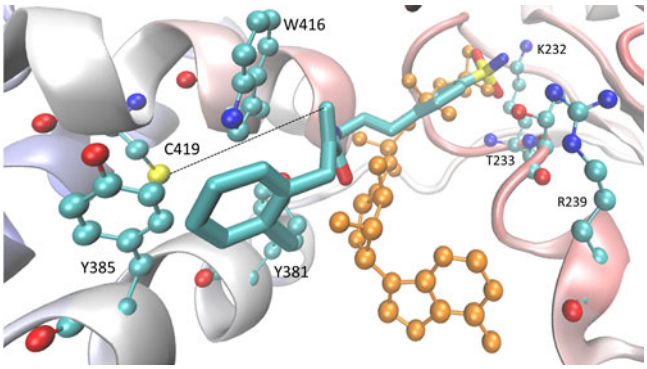

Figure 9. Comparison of the putative poses as computed for ATP (orange) and **14** (INF58, light blue). The dashed black line defines the path between the supposedly reactive Cys419 residue and the β-carbon atom of the acrylamide group.

Lastly, the ATP sugar moiety is engaged in H-bonds with Tyr381 and to a minor extent with Trp416.

As shown in Figure 9 (in light blue), compound **14** is accommodated in the regions of the binding site that harbor the ribose ring and the phosphate groups of ATP, where it can elicit a set of key interactions that can be schematized as follows.

The 2-chlorophenyl moiety is engaged in extended π–π stacking interactions with surrounding aromatic residues such as Tyr381, Tyr385, and Trp416. This last residue also contacts the reactive vinyl group of the acrylamide moiety and might have a key role in approaching the reactive ligand moiety to Cys419 (see below). The amide oxygen atom is involved in a clear H-bond with Tyr381, whereas the phenyl sulfonamide moiety mimics the ATP phosphate groups by stabilizing a rich set of charge-transfer interactions and reinforced H-bonds involving Lys232, Thr233, Arg237, and His522. Such an extended network of contacts should maintain the inhibitor in a pose stably conducive to the formation of a covalent adduct with the protein. In detail, the reactive acrylamide is surrounded by three rather close cysteine residues (i.e., Cys409, Cys415, and Cys419). Among them, Cys419 seems to be the most reactive one for two main reasons. First, it is the closest residue, as its distance to the acrylamide is 8.3 Å (the corresponding distances for Cys409 and Cys415 are 14.9 and 11.1 Å, respectively) and between Cys419 and the acrylamide there are no residues that can obstruct the approaching, whereas the hypothetic path for Cys409 and Cys415 is hindered by other residues as exemplified by Pro412. Second, Cys419 is surrounded by residues, such as Tyr385, which should enhance its reactivity by stabilizing its thiolate form with a mechanism already observed for albumin and glutathione transferase enzymes.[37]

The other simulated derivatives show similar poses and all are characterized by the capacity to insert the 2-chlorophenyl ring in the above-described subpocket lined by several aromatic residues that have the dual role of stabilizing the complex and of constraining the acrylamide moiety in a pose conducive to Michael addition. Notably, the obtained docking results and in particular the observed interactions stabilized by the varying moieties linked to the acrylamide nitrogen atom can offer additional explanations for the measured ATPase activity. Indeed, compounds **5**, **10**, and **12** reveal putative complexes that are very similar to that observed for **14**, in which the reinforced H-bonds with Lys232 and Arg237 are replaced by extended charge-transfer interactions with the distal phenyl ring in **5** and **10** and by H-bonds with the ester group in compound **12**.

Conclusions

With the aim to obtain covalent NLRP3 inhibitors, we designed and synthesized a series of acrylamide derivatives endowed with low intrinsic electrophilicity that was reflected in avoided unspecific idiosyncratic and cytotoxic effects. Most of the synthesized compounds prevented ATP-triggered, NLRP3-dependent pyroptotic cell death of PMA-differentiated THP-1 cells, moreover, they showed no significant cytotoxicity. The obtained results allowed the selection of 2-(2-chlorobenzyl)-*N*-phenethylacrylamide (**10**), methyl 4-[2-(2-chlorobenzyl)acrylamide]butanoate (**12**), and 2-(2-chlorobenzyl)-*N*-(4-sulfamoylphenethyl)acrylamide (**14**) able to prevent pyroptosis in a concentration-dependent manner and endowed with a promising pharmaco-toxicological profile. Derivatives **10**, **12**, and **14** were able to inhibit IL-1β release from different macrophage lines, with no effect on TLR-4 dependent TNF-α production. Compounds **10**, **12**, and **14** were also effective in inhibiting IL-1β release from macrophages bearing CAPS-associated NLRP3 mutants. Compound **14** (INF58) inhibited NLRP3 ATPase activity with an IC_{50} value of 74 μM, which resulted in a good hit compound to design new and improved direct NLRP3 inhibitors. In silico prediction of the binding mode of **14** in the ATPase catalytic pocket indicated that a putative interaction with the Cys419 residue might account for this activity. Binding studies to identify the binding site(s) of **14** (INF58) to human recombinant NLRP3 are in progress, and the results will be reported in due course.

Experimental Section

General procedures

All reactions were monitored by TLC on Merck 60 F_{254} (0.25 mm) plates, which were visualized by UV inspection and/or by spraying with $KMnO_4$ (0.5 g in 100 mL 0.1 N NaOH). Flash chromatography (FC) purifications were performed by using silica gel Fluka with 60 mesh particles. ^1H NMR and ^{13}C NMR spectra were registered with a Bruker Avance 300 spectrometer at 300 and 75 MHz, respectively. Coupling constants (*J*) are given in Hertz (Hz) and chemical shifts (δ) are given in ppm calibrated to tetramethylsilane as an internal standard. The following abbreviations are used to describe multiplicities: s = singlet, d = doublet, t = triplet, q = quadruplet, m = multiplet, and br = broad signal. Low-resolution mass spectra were recorded with a Finnigan-MAT TSQ700 in chemical ionization (CI) mode by using isobutane. Melting points were measured with a capillary apparatus (Büchi 540). The purities of the compounds were checked by UHPLC (PerkinElmer) Flexar 15, equipped with a UV/Vis diode array detector by using an Acquity UHPLC CSH Phenyl-Hexyl 1.7 μm 2.1 × 50 mm column (Waters) and H_2O/CH_3CN and H_2O/CH_3OH solvent systems. Detection was performed at λ =

200, 215, and 254 nm. The analytical data confirmed that the purities of the products were ≥95%.

Synthesis

Ethyl 2-{[(*tert*-butyldimethylsilyl)oxy](2-chlorophenyl)methyl}-acrylate (17): Imidazole (1.70 g, 25 mmol) was added to a stirred solution of **1**[22] (2.41 g, 10 mmol) in DMF (3 mL). After complete dissolution, *tert*-butyldimethylsilyl chloride (2.26 g, 15 mmol) was added portionwise, and the solution was stirred overnight at RT. Water (20 mL) was added, and the mixture was extracted with EtOAc (3×30 mL), washed with brine (30 mL), dried (Na_2SO_4), filtered, and concentrated under reduced pressure. Purification by silica gel chromatography (petroleum ether/EtOAc 9:1) gave **17** as a colorless oil (2.91 g, 82%): R_f=0.87 (petroleum ether/EtOAc 9:1); ^{1}H NMR (300 MHz, $CDCl_3$): δ=7.44–7.11 (m, 4H), 6.28 (s, 1H), 6.05 (s, 1H), 5.82 (s, 1H), 4.09 (q, J=7.1 Hz, 2H), 1.17 (t, J=7.1 Hz, 3H), 0.85 (s, 9H), 0.09 (s, 3H) −0.12 ppm (s, 3H); ^{13}C NMR (75 MHz, $CDCl_3$): δ=168.5, 146.2, 142.9, 135.6, 132.2, 132.1, 131.5, 129.6, 127.9, 71.9, 63.5, 28.6, 21.0, 17.0, −2.0, −2.1 ppm; MS (CI, isobutane): *m/z* (%): 357 (32), 355 (100) $[M+H]^+$.

2-{[(*tert*-Butyldimethylsilyl)oxy](2-chlorophenyl)methyl}acrylic acid (18): LiOH (1.96 g, 82.0 mmol) was added to a solution of compound **17** (2.91 g, 8.20 mmol) in CH_3CN/H_2O (1:1, 20 mL). The mixture was stirred at 60 °C overnight. The solvent was evaporated under reduced pressure. The residue was diluted with 1 N HCl (10 mL) and extracted with EtOAc (4×25 mL). The combined organic phase was washed with brine (30 mL), dried (Na_2SO_4), filtered, and concentrated under reduced pressure. Purification by silica gel chromatography (CH_2Cl_2/MeOH 97:3 to 9:1) gave **18** as a colorless oil (2.28 g, 85%): R_f=0.68 (CH_2Cl_2/MeOH 9:1); ^{1}H NMR (300 MHz, $CDCl_3$): δ=10.04 (br, 1H), 7.50 (d, J=7.8 Hz, 1H), 7.32–7.16 (m, 3H), 6.42 (s, 1H), 6.03 (s, 1H), 5.85 (s, 1H), 0.87 (s, 9H), 0.10 (s, 3H), −0.09 ppm (s, 3H); ^{13}C NMR (75 MHz, $CDCl_3$): δ= 171.2, 142.9, 140.2, 133.3, 130.0, 129.7, 129.4, 128.6, 127.4, 69.5, 26.4, 28.8, −4.2, −4.3 ppm; MS (CI, isobutane): *m/z* (%): 329 (37), 327 (100) $[M+H]^+$.

General procedure for the synthesis of compounds 19a–d: Carboxylic acid **18** (0.456 mg, 1.39 mmol) was dissolved in THF (10 mL); then, DIPEA (0.364 mL, 2.10 mmol) and DCC (0.288 g, 1.39 mmol) were added. The mixture was stirred for 15 min at 0 °C and then at RT for another 2 h. The amine (2 equiv) was then added, and the mixture was stirred at RT overnight. The mixture was filtered, and the liquid phase was extracted with EtOAc (4× 30 mL). The organic phase was washed with saturated NH_4Cl solution (20 mL), dried (Na_2SO_4), filtered, and concentrated. The product was purified by silica gel chromatography (petroleum ether/EtOAc 9:1).

2-{[(*tert*-Butyldimethylsilyl)oxy](2-chlorophenyl)methyl}-*N*-propylacrylamide (19a): The reaction was run with propylamine (0.228 mL, 2.78 mmol) to obtain **19a** as a colorless oil (0.317 g, 62%): R_f=0.74 (petroleum ether/EtOAc 8:2); ^{1}H NMR (300 MHz, $CDCl_3$): δ=7.55 (d, J=7.8 Hz,1H),7.29–7.19 (m, 3H), 6.68 (br, 1H), 5.95 (s, 1H), 5.92 (s, 1H), 5.53 (s, 1H), 3.24–3.21 (m, 2H), 1.55–1.48 (m, 2H), 0.90 (s, 9H), 0.87 (t, J=7.1 Hz, 3H), 0.12 (s, 3H), −0.02 ppm (s, 3H); ^{13}C NMR (75 MHz, $CDCl_3$): δ=166.6, 144.4, 138.9, 132.2, 129.6, 128.8, 128.3, 126.7, 121.6, 72.1, 41.1, 25.7, 22.8, 18.1, 11.5, 0.0, −5.0 ppm; MS (CI, isobutane): *m/z* (%): 370 (32), 368 (100) $[M+H]^+$.

2-{[(*tert*-Butyldimethylsilyl)oxy](2-chlorophenyl)methyl}-*N*-cyclohexylacrylamide (19b): The reaction was run with cyclohexylamine (0.190 mL, 2.78 mmol) to obtain **19b** as a pale-yellow oil (0.420 g, 74%): R_f=0.72 (petroleum ether/EtOAc 9:1); ^{1}H NMR (300 MHz, $CDCl_3$): δ=7.67 (d, J=7.6 Hz, 1H), 7.35–7.23 (m, 3H), 6.26 (br, 1H), 5.85 (s, 1H), 5.76 (s, 1H), 5.33 (s, 1H), 1.93–1.83 (m, 2H), 1.75–1.58 (m, 3H), 1.41–1.32 (m, 2H), 1.22–1.13 (m, 4H), 0.96 (s, 9H), 0.24 (s, 3H), −0.21 ppm (s, 3H); ^{13}C NMR (75 MHz, $CDCl_3$): δ=168.6, 144.8, 141.9, 131.2, 129.4, 128.5, 128.0, 127.1, 122.6, 74.1, 51.6, 43.3, 31.0, 25.9, 25.7, 24.0, −0.5, −4.0 ppm; MS (CI, isobutane): *m/z* (%): 410 (32), 408 (100) $[M+H]^+$.

***N*-Benzyl-2-{[(*tert*-butyldimethylsilyl)oxy](2-chlorophenyl)methyl}acrylamide (19c)**: The reaction was run with benzylamine (0.304 mL, 2.78 mmol) to obtain **19c** as a pale-yellow oil (0.468 g, 81%): R_f=0.70 (petroleum ether/EtOAc 9:1); ^{1}H NMR (300 MHz, $CDCl_3$): δ=7.39–7.15 (m, 9H), 6.23 (br, 1H), 5.79 (s,1H), 5.31 (s, 1H), 5.18 (s, 1H), 3.87 (s, 2H), 0.94 (s, 9H), 0.22 (s, 3H), −0.33 ppm (s, 3H); ^{13}C NMR (75 MHz, $CDCl_3$): δ=168.2, 143.1, 138.9, 136.3, 134.6, 131.5, 130.0, 129.1, 128.4, 128.0, 127.8, 127.3, 121.1, 73.8, 44.1, 32.0, 25.7, −1.5, −3.9 ppm; MS (CI, isobutane): *m/z* (%): 418 (32), 416 (100) $[M+H]^+$.

***tert*-Butyl [3-(2-{[(*tert*-butyldimethylsilyl)oxy](2-chlorophenyl)methyl}acrylamido)propyl]carbamate (19d)**: The reaction was run with *N*-Boc-1,3-propanediamine (0.484 g, 2.78 mmol) to obtain **19d** as a off-white oil (0.403 g, 60%): R_f=0.61 (petroleum ether/EtOAc 9:1); ^{1}H NMR (300 MHz, $CDCl_3$): δ=7.35–7.13 (m, 4H), 7.03 (br, 1H), 5.79 (s,1H), 5.63 (s, 1H), 5.25 (br, 1H), 5.10 (s, 1H), 3.33 (t, J= 7.1 Hz, 2H), 3.08 (t, J=8.1 Hz, 2H), 1.61–1.57 (m, 2H), 1.42 (s, 9H), 0.96 (s, 9H), 0.18 (s, 3H), −0.32 ppm (s, 3H); ^{13}C NMR (75 MHz, $CDCl_3$): δ=168.7, 156.6, 142.4, 136.3, 134.0, 131.1, 129.5, 128.0, 126.7, 119.7, 79.2, 74.2, 37.0, 36.3, 31.1, 30.0, 28.5, 25.7, −1.5, −3.8 ppm; MS (CI, isobutane): *m/z* (%): 485 (32), 483 (100) $[M+H]^+$.

General procedure for synthesis of compounds 4–7: Tetrabutylammonium fluoride (1.0 M in THF, 0.77 mL, 0.77 mmol) was added to a solution of compound **19a–d** (0.70 mmol) in dry THF (5 mL) at 0 °C. The mixture was stirred at RT for 1 h and then diluted with water (15 mL) and extracted with CH_2Cl_2 (3×20 mL). The organic phase was washed with brine (20 mL) and water (20 mL), dried (Na_2SO_4), filtered, and concentrated. The products were purified by silica gel chromatography (petroleum ether/EtOAc 95:5).

2-[(2-Chlorophenyl)(hydroxy)methyl]-*N*-propylacrylamide (4): Obtained as a white solid (0.169 g, 95%) starting from **19a**: characterization data were in agreement with the previously reported data.[20]

***N*-Benzyl-2-[(2-chlorophenyl)(hydroxy)methyl]acrylamide (5)**: Obtained as a white solid (0.169 g, 80%) starting from **19b**: R_f=0.52 (petroleum ether/EtOAc 85:15); mp: 94.3–95.6 °C; ^{1}H NMR (300 MHz, $CDCl_3$): δ=7.63 (d, J=7.6 Hz, 1H), 7.33–7.14 (m, 8H), 6.78 (br, 1H), 5.85 (d, J=4.9 Hz, 1H), 5.78 (s, 1H), 5.30 (s, 1H), 3.57 (d,, J=5.1 Hz,1H), 3.16 ppm (s, 2H); ^{13}C NMR (75 MHz, $CDCl_3$): δ= 168.4, 143.2, 138.5, 136.6, 134.8, 131.7, 129.9, 129.1, 128.6, 128.1, 127.7, 127.4, 120.1, 66.7, 44.0 ppm; MS (CI, isobutane): *m/z* (%): 304 (32), 302 (100) $[M+H]^+$.

2-[(2-Chlorophenyl)(hydroxy)methyl]-*N*-cyclohexylacrylamide (6): Obtained as a white solid (0.179 g, 87%) starting from **19c**: R_f= 0.41 (petroleum ether/EtOAc 9:1); mp: 119.4–120.8 °C; ^{1}H NMR (300 MHz, $CDCl_3$): δ=7.69 (d, J=7.6 Hz, 1H), 7.34-.7.23 (m, 3H), 6.27 (br, 1H), 5.84 (s, 1H), 5.76 (s, 1H), 5.30 (s, 1H), 4.28 (br, 1H), 1.94–1.87(m, 2H), 1.75–1.60 (m, 3H), 1.41–1.32 (m, 2H), 1.22–1.13 ppm (m, 4H); ^{13}C NMR (75 MHz, $CDCl_3$): δ=168.6, 144.6, 142.1,

131.2, 129.3, 128.3, 127.7, 127.0, 122.3, 66.7, 51.5, 43.3, 25.7, 24.2 ppm; MS (CI, isobutane): *m/z* (%): 296 (32), 294 (100) $[M+H]^+$.

3-{2-[(2-Chlorophenyl)(hydroxy)methyl]acrylamido}propan-1-aminium 2,2,2-trifluoroacetate (7): Trifluoroacetic acid (0.500 mL, 6.49 mmol) was added dropwise to a solution of **19d** in CH_2Cl_2 (5 mL). The mixture was stirred at RT for 2 h and then concentrated to dryness. The white solid was washed several times with CH_2Cl_2 (2×20 mL) and diethyl ether (3×20 mL), and **7** was obtained as a white amorphous solid (140.6 mg, 99%); ^{1}H NMR (300 MHz, D_2O): δ = 7.47–7.29 (m, 4H), 5.83 (s,1H), 5.76 (s, 1H), 5.26 (s, 1H), 3.17–3.11 (m, 2H), 2.71 (t, J = 7.1 Hz, 2H), 1.69–1.55 ppm (m, 2H); ^{13}C NMR (75 MHz, D_2O): δ = 172.5, 142.2, 136.1, 134.1, 131.3, 129.9, 128.7, 127.5, 121.2, 118.5, 114.8, 68.9, 40.5, 34.4, 26.9 ppm.

Ethyl 3-(2-chlorophenyl)-2-(diethoxyphosphoryl)propanoate (20): 60% NaH in mineral oil (1.64 g, 41.0 mmol) was added to a stirred solution of ethyl (diethoxyphosphoryl)acetate (7.86 g, 35.1 mmol) in DMF (30 mL) at 0 °C, and the mixture was stirred at 0 °C for 1 h. Then, 2-chlorophenylmethyl bromide (6.00 g, 29.3 mmol) was added at 0 °C, and the mixture was stirred at RT for 18 h. The reaction was quenched with water, and the mixture was extracted with EtOAc (50 mL×3). The combined organic layer was washed with water (50 mL) and brine (50 mL), dried (Na_2SO_4), and concentrated. Purification by silica gel chromatography (petroleum ether/EtOAc from 7:3 to 1:1) gave **20** as a colorless oil (7.25 g, 71%): R_f = 0.29 (petroleum ether/EtOAc 7:3); ^{1}H NMR (300 MHz, $CDCl_3$): δ = 7.36–7.09 (m, 4H), 4.26–4.06 (m, 6H), 3.52–3.27 (m, 3H), 1.39–1.33 (m, 6H), 1.15 ppm (t, J = 7.0 Hz, 3H).[38]

Ethyl 2-(2-chlorobenzyl)acrylate (21): A solution of potassium carbonate (8.62 g, 62.4 mmol) in water (60 mL) was added to a stirred mixture of **20** (7.25 g, 20.8 mmol) and paraformaldehyde (4.13 g, 137 mmol) in water (60 mL) at RT. The mixture was stirred at 90 °C overnight. After cooling to RT, the mixture was extracted with EtOAc (3×50 mL), and the organic layer was washed with brine (50 mL), dried (Na_2SO_4), filtered, and concentrated. Purification by silica gel chromatography (petroleum ether/EtOAc 7:3) gave **21** as a colorless oil (3.06 g, 66%): R_f = 0.45 (petroleum ether/EtOAc 95:5); ^{1}H NMR (300 MHz, $CDCl_3$): δ = 7.50–6.99 (m, 4H), 6.27 (d, J = 0.9 Hz,1H), 5.33 (d, J = 1.2 Hz, 1H), 4.22 (q, J = 7.1 Hz, 2H), 3.76 (s, 2H), 1.29 ppm (t, J = 7.1 Hz, 3H); ^{13}C NMR (75 MHz, $CDCl_3$): δ = 166.8, 138.4, 136.4, 134.5, 131.2, 129.6, 127.9, 126.8, 126.3, 60.4, 35.4, 14.2 ppm; MS (CI, isobutane): *m/z* (%): 227 (32), 225 (100) $[M+H]^+$.

2-(2-Chlorobenzyl)acrylic acid (22): 2.5 M NaOH (1.3 mL) was added to a stirred solution of **21** (3.06 g, 19.6 mmol) in EtOH (5 mL), and the mixture was stirred at RT overnight. The mixture was diluted with 10% $NaHCO_3$ (15 mL) and extracted with EtOAc (15 mL). The aqueous phase was acidified with 1 M HCl (to pH < 1) and then extracted with EtOAc (3×20 mL). The organic phase was dried (Na_2SO_4), filtered, and concentrated. Compound **22** was obtained as a white solid (2.54 g, 95%): mp: 90.5–91.5 °C; ^{1}H NMR (300 MHz, $CDCl_3$): δ = 11.84 (br, 1H),7.37–7.14 (m, 4H), 6.41 (s,1H), 5.44 (s, 1H), 3.74 ppm (s, 2H); ^{13}C NMR (75 MHz, $CDCl_3$): δ = 172.4, 137.9, 136.5, 134.9, 131.6, 130.1, 129.4, 128.5, 127.3, 35.4 ppm; MS (CI, isobutane): *m/z* (%): 199 (32), 197 (100) $[M+H]^+$.

2,5-Dioxopyrrolidin-1-yl-2-(2-chlorobenzyl)acrylate (23): *N,N′*-Dicyclohexylcarbodiimide (2.50 g, 12.1 mmol) was added to a stirred solution of **22** (2.39 g, 12.1 mmol) in dry THF (25 mL) at 0 °C. After 10 min, *N*-hydroxysuccinimide (1.39 g, 12.1 mmol) was added at the same temperature, and the mixture was stirred at RT overnight. The mixture was filtered, and the liquid phase was extracted with EtOAc (3×30 mL). The organic layer was washed with saturated NH_4Cl solution (15 mL), dried (Na_2SO_4), filtered, and concentrated. Purification by silica gel chromatography (CH_2Cl_2/EtOAc 99:1) gave **23** as a white solid (3.00 g, 84%): R_f = 0.37 (CH_2Cl_2/EtOAc 99:1); mp: 131.7–133.2 °C; ^{1}H NMR (300 MHz, $CDCl_3$): δ = 7.38–7.18 (m, 4H), 6.55 (s, 1H), 5.62 (s, 1H), 3.80 (s, 2H), 2.82 ppm (s, 4H); ^{13}C NMR (75 MHz, $CDCl_3$): δ = 169.7, 135.3, 134.9, 134.2, 131.6, 130.3, 130.1, 129.4, 128.5, 127.3, 35.7, 26.0 ppm; MS (CI, isobutane): *m/z* (%): 296 (32), 294 (100) $[M+H]^+$.

General procedure for the synthesis of compounds 8–14: The amine (2.00 mmol) was added to a stirred solution of **23** (0.29 g, 1.00 mmol) in CH_2Cl_2/DMF (2:1, 6 mL) at RT; this was followed by the addition of triethylamine (3.00 mmol). The mixture was stirred at RT for 2 h-24 h. The mixture was diluted with water (30 mL), acidified with 1 N HCl (20 mL), and then extracted with EtOAc (4×30 mL). The organic phase was washed with brine (35 mL), dried (Na_2SO_4), filtered, and concentrated to obtain the crude product.

2-(2-Chlorobenzyl)-*N*-propylacrylamide (8): Propylamine (118.2 mg, 2.00 mmol) was used as the amine, and the mixture was stirred for 6 h. Purification by silica gel chromatography (CH_2Cl_2 to CH_2Cl_2/EtOAc 99:1) gave **8** as a pale-yellow oil (183.5 mg, 77%): R_f = 0.63 (CH_2Cl_2/EtOAc 9:1); ^{1}H NMR (300 MHz, $CDCl_3$): δ = 7.37–7.17 (m, 4H) 5.92 (br, 1H), 5.71 (s,1H), 5.11 (s, 1H), 3.78 (s, 2H), 3.24 (t, J = 7.1 Hz, 2H), 1.51 (m, 2H), 0.87 ppm (t, J = 7.2 Hz, 2H); ^{13}C NMR (75 MHz, $CDCl_3$): δ = 166.9, 140.4, 137.3, 134.3, 128.6, 128.5, 127.2, 126.9, 124.3, 40.8, 37.1, 23.2, 11.2 ppm; MS (CI, isobutane): *m/z* (%): 240 (32), 238 (100) $[M+H]^+$.

***N*-Benzyl-2-(2-chlorobenzyl)acrylamide (9)**: Benzylamine (214.3 mg, 2.00 mmol) was used as the amine, and the mixture was stirred for 8 h. Purification by silica gel chromatography (CH_2Cl_2 to CH_2Cl_2/EtOAc 98:2) gave **9** as a white solid (157.2 mg, 56%): R_f = 0.81 (CH_2Cl_2/EtOAc 9:1); mp: 87.1–88.0 °C; ^{1}H NMR (300 MHz, $CDCl_3$): δ = 7.38–7.21 (m, 9H), 6.23 (br, 1H), 5.76 (s,1H), 5.18 (s, 1H), 4.50 (s, 2H), 3.84 (s, 2H); ^{13}C NMR (75 MHz, $CDCl_3$): δ = 168.4, 143.2, 138.5, 136.4, 134.8, 131.7, 130.0, 129.1, 128.5, 128.1, 127.9, 127.4, 120.1, 44.1, 36.3 ppm; MS (CI, isobutane): *m/z* (%): 288 (32), 286 (100) $[M+H]^+$.

2-(2-Chlorobenzyl)-*N*-phenethylacrylamide (10): Phenethylamine (242.4 mg, 2.00 mmol) was used as the amine, and the mixture was stirred for 12 h. Purification by silica gel chromatography (CH_2Cl_2/EtOAc 9:1) gave **10** as a white solid (158.9 mg, 53%): R_f = 0.71 (CH_2Cl_2/EtOAc 9:1); mp: 66.5–68.0 °C; ^{1}H NMR (300 MHz, $CDCl_3$): δ = 7.34–7.09 (m, 9H), 5.90 (br, 1H), 5.61 (s, 1H), 5.07 (s,1H), 3.73 (s, 2H), 3.52 ppm (t, J = 7.1 Hz, 2H), 2.78 ppm (t, J = 7.1 Hz, 2H); ^{13}C NMR (75 MHz, $CDCl_3$): δ = 168.8, 140.2, 139.3, 137.4, 134.2, 130.6, 129.3, 128.7, 128.5, 127.7, 127.2, 125.9, 124.2, 40.8, 37.1, 35.2 ppm; MS (CI, isobutane): *m/z* (%): 302 (32), 300 (100) $[M+H]^+$.

***N*-(3-Aminopropyl)-2-(2-chlorobenzyl)acrylamide trifluoroacetate (11)**: *tert*-Butyl (3-aminopropyl)carbamate (348.5 mg, 2.00 mmol) was used as the amine, and the mixture was stirred for 3 h. Purification by silica gel chromatography (petroleum ether/EtOAc 1:1) gave Boc-protected **11** as a white solid (264.7 mg, 75%). This intermediate (148.7 mg, 0.422 mmol) was dissolved in CH_2Cl_2 (5 mL) and trifluoroacetic acid (0.500 mL, 6.49 mmol) was added. The mixture was stirred at RT for 1 h and then concentrated to dryness. The white solid was washed several times with CH_2Cl_2 (2×20 mL) and diethyl ether (3×20 mL), and **11** was obtained as a white crystalline solid (134.5 mg, 87%): R_f = 0.23 (CH_2Cl_2/MeOH 1:1); mp: 118.1–119.0 °C; ^{1}H NMR (300 MHz, D_2O): δ = 7.30 (d, J = 7.5 Hz, 1H), 7.13–7.10 (m, 3H), 5.54 (s,1H), 5.24 (s, 1H), 3.61 (s, 2H), 3.11 (t, J = 6.5 Hz, 2H), 2.54 (t, J = 6.6 Hz, 2H), 1.67–1.55 (m, 2H), 1.66–1.50 (m, 4H), 1.23–0.87 ppm (m, 6H); ^{13}C NMR (75 MHz, D_2O): δ = 172.5,

142.2, 136.1, 134.1, 131.3, 129.9, 128.7, 127.5, 121.2, 118.5, 114.8, 40.5, 36.6, 34.4, 26.9 ppm.

Methyl 4-[2-(2-chlorobenzyl)acrylamido]butanoate (12): Methyl 4-aminobutanoate hydrochloride (307.2 mg, 2.00 mmol) was used as the amine, and the mixture was stirred for 16 h. Purification by silica gel chromatography (petroleum ether/EtOAc 7:3 to 1:1) gave **12** as a white solid (162.7 mg, 55%): R_f = 0.64 (petroleum ether/EtOAc 1:1); mp: 69.5–71.0 °C; ^{1}H NMR (300 MHz, $CDCl_3$): δ = 7.38–7.18 (m, 4H), 6.16 (br, 1H), 5.72 (s,1H), 5.12 (s, 1H), 3.77 (s, 2H), 3.67 (s, 3H), 3.34 (t, J = 7.1 Hz, 2H), 2.32 (t, J = 7.1 Hz, 2H), 1.88–1.79 ppm (m, 2H); ^{13}C NMR (75 MHz, $CDCl_3$): δ = 174.4, 168.6, 143.2, 136.5, 134.7, 131.6, 130.0, 128.5, 127.4, 119.9, 52.2, 39.6, 36.2, 31.9, 24.8 ppm; MS (CI, isobutane): *m/z* (%): 298 (32), 296 (100) $[M+H]^+$.

4-[2-(2-Chlorobenzyl)acrylamido]butanoic acid (13): 4-Aminobutanoic acid (206.2 mg, 2.00 mmol) was used as the amine, and the mixture was stirred in CH_2Cl_2/DMF (1:1, 10 mL) for 24 h. Purification by silica gel chromatography (CH_2Cl_2/MeOH 99:1) gave **13** as a white solid (128.9 mg, 66%): R_f = 0.80 (CH_2Cl_2/MeOH 1:1); mp: 68.5–70.3 °C; ^{1}H NMR (300 MHz, $CDCl_3$): δ = 10.60 (br, 1H), 7.33–7.17 (m, 4H), 6.56 (br, 1H), 5.72 (s, 1H), 5.09 (s, 1H), 3.73 (s, 2H), 3.32 (t, J = 7.1 Hz, 2H), 2.31 (t, J = 7.1 Hz, 2H), 1.85–1.76 ppm (m, 2H); ^{13}C NMR (75 MHz, $CDCl_3$): δ = 178.2, 168.3, 142.7, 136.4, 134.7, 131.6, 130.0, 128.6, 127.4, 120.5, 39.6, 36.1, 31.9, 24.7 ppm.

2-(2-Chlorobenzyl)-*N*-(4-sulfamoylphenethyl)acrylamide (14): 4-(2-Aminoethyl)-benzenesulfonamide (400.5 mg, 2.00 mmol) was used as the amine, and the mixture was stirred in DMF (10 mL) for 12 h. Purification by silica gel chromatography (CH_2Cl_2 to CH_2Cl_2/EtOAc 7:3) gave **14** as a white solid (223.5 mg, 59%): R_f = 0.43 (CH_2Cl_2/EtOAc 1:1); mp: 150.3–151.1 °C; ^{1}H NMR (300 MHz, CD_3OD): δ = 7.79 (d, J = 8.0 Hz, 2H), 7.44–7.28 (m, 4H), 7.22 (d, J = 9.1 Hz, 2H), 5.66 (s,1H), 5.11 (s, 1H), 3.72 (s, 2H), 3.47 (t, J = 7.1 Hz, 2H), 2.88 ppm (t, J = 7.1 Hz, 2H); ^{13}C NMR (75 MHz, CD_3OD): δ = 168.5, 142.9, 141.6, 140.4, 135.0, 132.9, 129.7, 128.0, 127.9, 126.8, 125.6, 124.7, 117.9, 39.2, 34.2, 33.5 ppm; MS (CI, isobutane): *m/z* (%): 381 (32), 379 (100) $[M+H]^+$.

2-(2-Chlorobenzyl)-*N*-{4-[*N*-(cyclohexylcarbamoyl)sulfamoyl]phenethyl}acrylamide (15): Compound **14** (98.7 mg, 0.261 mmol) was dissolved in dry acetone (15 mL) under a N_2 atmosphere and K_2CO_3 (108.0 mg, 0.732 mmol) was added portionwise. After stirring at reflux for 1.5 h, cyclohexyl isocyanate (52.0 mg, 0.417 mmol) dissolved in dry acetone (20 mL) was added dropwise to the mixture. The mixture was heated at reflux overnight. After cooling, water (15 mL) was added, and the mixture was acidified to pH 1 with 1 N HCl. The obtained white precipitate was collected and recrystallized from methanol to afford **15** as a white solid (51.0 mg, 39%): R_f = 0.43 (CH_2Cl_2/EtOAc 1:1); mp: 166.7–168.5 °C; ^{1}H NMR (300 MHz, [D_6]DMSO): δ = 10.34 (br, 1H), 8.25 (s, 1H), 7.79 (d, J = 8.0 Hz, 2H) 7.44–7.28 (m, 6H), 6.39 (d, J = 7.7 Hz, 1H), 5.69 (s,1H), 5.03 (s, 1H), 3.65 (s, 2H), 3.38 (t, J = 6.9 Hz, 2H), 3.33–3.30 (m, 1H), 2.84 (t, J = 6.8 Hz, 2H), 1.66–1.50 (m, 4H), 1.23–0.87 ppm (m, 6H); ^{13}C NMR (75 MHz, [D_6]DMSO): δ = 168.1, 150.5, 146.1, 139.0, 137.4, 134.2, 131.9, 130.1, 129.9, 129.1, 128.1, 128.0, 127.7, 120.0, 48.9, 40.7, 36.1, 35.5, 33.2, 22.8, 25.1 ppm; MS (CI, isobutane): *m/z* (%): 505 (32), 503 (100) $[M+H]^+$.

***N,N'*-(Propane-1,3-diyl)bis[2-(2-chlorobenzyl)acrylamide] (16)**: DIPEA (51 μL, 0.299 mmol) was added dropwise to a solution of **11** (91.0 mg, 0.249 mmol) in DMF (5 mL). The mixture was stirred at RT for 10 min and then **23** (61.0 mg, 0.208 mmol) was added. The mixture was stirred at RT for 1 h. The mixture was diluted with 1 N HCl (10 mL) and extracted with CH_2Cl_2 (3×25 mL). The organic phase was dried (Na_2SO_4), filtered, and concentrated under reduced pressure. Purification by silica gel chromatography (CH_2Cl_2/MeOH 98:2) gave **16** as a white solid (75.0 mg, 84%): R_f = 0.30 (CH_2Cl_2/MeOH 98:2); mp: 138.8–140.3 °C; ^{1}H NMR (300 MHz, $CDCl_3$): δ = 7.61–6.94 (m, 8H), 6.61 (br, 2H), 5.79 (s, 2H), 5.17 (s, 2H), 3.69 (s, 4H), 3.19 (t, J = 6.2 Hz, 4H), 1.67–1.46 ppm (m, 2H); ^{13}C NMR (75 MHz, $CDCl_3$): δ = 168.7, 142.7, 136.1, 134.4, 131.2, 129.6, 128.1, 126.9, 119.7, 35.9, 35.5, 29.5 ppm; MS (CI, isobutane): *m/z* (%): 432 (64), 430 (100) $[M+H]^+$.

Kinetic cysteamine chemoassay: The thiol assay was performed in 96-well plates by using 100 mM phosphate buffer (pH 7.4) with 500 μM ethylenediaminetetraacetic acid (EDTA) as the solvent system. The DTNB reagent was prepared by dissolving DTNB (0.014 mmol, Sigma–Aldrich, St. Louis, MO, USA) and sodium hydrogen carbonate (0.5 mmol) in 100 mM phosphate buffer (pH 7.2, 25 mL). All measurements were done with a Multilabel Plate Reader (Victor X4, PerkinElmer, Waltham, MA, USA) at 37 °C. To perform the assay, CH_3CN solutions of the compounds (10 mM) and a water solution of cysteamine (CAM) (Sigma–Aldrich) (10 mM) were diluted in the phosphate buffer to give a concentration of 0.5 mM. Equal amounts of both solutions were combined and mixed, and the kinetic measurements were started immediately. At various time points (over a time of 90 min), the DTNB reagent (150 μL) was added, and after 1 min the absorption at λ = 405 nm was measured. The concentration of the remaining reduced CAM was determined by a CAM calibration curve of thiol content versus absorbance (CAM concentration ranging from 0.03 to 0.35 mM). Rate constants of the reaction between CAM and the electrophilic compounds were determined as reported.[22]

Reaction of compound 14 with cysteamine: The electrophilic reactivity of compound **14** was quantified in terms of the pseudo-first-order reaction rate constant, $k_{pseudo1st}$, by employing cysteamine (CAM) as a nucleophile. The reaction vessel contained 500 μM electrophile and 5 mM CAM in 100 mM potassium phosphate buffer (pH 7.4) with 25% acetonitrile as co-solvent. The stirred mixture was maintained at (37 ± 0.5) °C for 7 h. At different time intervals, an aliquot (500 μL) of this solution was analyzed by reversed-phase UHPLC by using a Flexar UHPLC (PerkinElmer) equipped with a Flexar Solvent Manager 3-CH-Degasser, a Flexar-FX UHPLC autosampler, a Flexar-FX PDA UHPLC detector, a Flexar-LC column oven, and a Flexar-FX-15 UHPLC pump. The analytical column was an Acquity CSH (2.1×100 mm, 1.7 μm particle size) (Waters) column. The samples were analyzed by using an isocratic method by employing a mobile phase consisting of methanol/buffer (70:30, flow rate 0.2 mL min^{-1}). The column effluent was monitored at λ = 204 nm referenced against λ = 360 nm. Quantification was done by using calibration curves of compound **14** chromatographed under the same conditions. The linearity of the calibration curves was determined in the concentration range of 100 to 1000 μM (r^2 > 0.98). Data analysis was performed by using Chromera Manager (PerkinElmer). All experiments were run in triplicate. The pseudo-first-order rate constant was determined by plotting the natural log of the concentration of **14** as a function of time. The negative slope of the straight line is the pseudo-first-order rate constant. The value of $k_{pseudo1st}$ was then calculated according to the reported method.[29]

Albumin modification test: The analytic platform was composed of a Surveyor LC system, which was connected to a TSQ Quantum Ultra mass spectrometer through a Finnigan IonMax electrospray ionization (ESI) source assembled with a low flow stainless steel emitter (Thermo Fisher Scientific, Rodano, MI, Italy). Each compound was dissolved in acetonitrile and tested separately. Compounds were spiked into fresh human serum down to a concentra-

tion of 1 mM. The spiked volume was less than 10% of serum volume to avoid protein precipitation. The temperature was kept at 37 °C throughout the incubation time (3 h). Before the analysis, serum aliquots were diluted 200-fold into $H_2O/CH_3CN/HCO_2H$ (70:30:0.1 *v/v/v*). Samples were then centrifuged for 10 min at 18000 g, and the supernatant was placed in clear glass vials and kept at 4 °C in the autosampler compartment. The analyses were performed by an automated loop injection method, and sampling was programmed as a 50 μL-partial-loop injection performed by the HPLC system. Once loaded into the sample loop, samples were pushed at a flow rate of 25 μL min^{-1} through a peek tube directly connected to the ESI source. The mobile phase isocratic flow was delivered by the pump at the final composition $H_2O/CH_3CN/HCO_2H$ (70:30:0.1 *v/v/v*). The analyzer was operating under conditions similar to those reported.[27] Briefly, MS spectra were acquired for 5 min by a TSQ Quantum Ultra mass spectrometer in positive-ion mode by using the following settings: ESI voltage, 3.5 KV; capillary temperature, 300 °C; sheath gas, 35%; Q3 scan range, $m/z = 1410–1500$; Q3 power, 0.4 amu; scan time, 1 s; Q2 gas pressure, 200 Pa; skimmer offset, 10 V; microscan set to 3. Full instrument control and extraction of albumin ESI mass spectra were provided by Xcalibur software (version 2.0.7, Thermo Fisher Scientific, Rodano, MI, Italy). Mass spectra deconvolution was provided by MagTran software (version 1.02).[39] Covalent adducts were detected by the expected molecular weights [i.e., M_r(adduct) = M_r(albumin) + M_r(compound)]. The amount of modified albumin was then calculated from the relative abundance of unmodified protein and adducts.

Biological studies

In vitro models of pyroptosis: Pyroptosis was studied as previously described.[22] The day before each experiment, cells were plated in 48-well culture plates (75×10^3 cells well^{-1}) and were differentiated into monocyte-macrophages-like cells by treatment with PMA (50 nM; 24 h; Sigma–Aldrich). PMA-differentiated THP-1 cells were washed with phosphate-buffered saline (PBS, 2×) and primed with LPS (5 μg mL^{-1}; 4 h; Sigma–Aldrich) in serum-free medium. Cell death was triggered with ATP (5 mM; 1 h; Sigma–Aldrich). Cell death was quantified by using the CytoTox 96 Non-Radioactive Cytotoxicity Assay (Promega Corporation, Madison, MI, USA), based on a colorimetric measurement of LDH activity in the collected supernatants. Cell death was expressed according to the manufacturer's instruction.

Cytotoxicity assay: THP-1 cells were plated in 96-well culture plates (5×10^3 cells well^{-1}) and exposed to increasing concentrations (0.1–100 μM) of each compound. The cultures were maintained at 37 °C, 95% air/5% CO_2 in a fully humidified incubator. Cell viability was measured at 72 h by 3-(4,5-dimethylthiazol-2-yl)-2,5-diphenyltetrazolium bromide (MTT) assay.

Mice: C57Bl/6J mice were housed at the PBES Facility (ENS Lyon). Experiments were performed in accordance with European and institutional guidelines. Inflammatory peritoneal macrophages were elicited by the intraperitoneal injection of 4% thioglycolate broth for 4 days.

Constructs: Mouse NLRP3 cDNA was amplified by PCR from cDNAs of C57Bl/6J mouse macrophages. cDNAs coding for R258W, A350V, and L351P NLRP3 mutants were obtained from mouse NLRP3 cDNA by PCR (QuickChange II site-directed mutagenesis kit, Agilent Technologies) by using the following oligonucleotides:

mNLRP3_R258W_F: ctatttgttctttatccactgctgggaggtgagcctcaggac,

mNLRP3_R258W_R: gtcctgaggctcacctcccagcagtggataaagaacaaatag,

mNLRP3_A350V_F: cataacgacgaggccggtagtcttggagaaactgcagcatc,

mNLRP3_A350V_R: gatgctgcagtttctccaagactaccggcctcgtcgttatg,

mNLRP3_L351P_F: cgacgaggccggtagccccggagaaactgcagcatctc,

mNLRP3_L351P_R: gagatgctgcagtttctccggggctaccggcctcgtcg.

WT, R258W, A350V, and L351P NLRP3 cDNAs were cloned in GFP encoding pInducer21 under a doxycycline-dependent promotor for lentiviral vector production.

Cell culture: Immortalized wild-type and NLRP3 KO bone-marrow-derived macrophages (BMDMs) were a kind gift from Dr. E. Alnemri (Thomas Jefferson University). Immortalized NLRP3 KO BMDMs were reconstituted with WT, R258W, A350V, or L351P NLRP3 by lentiviral transduction followed by flow cytometry sorting of green fluorescent protein (GFP)-positive cells. Inflammatory peritoneal macrophages and immortalized BMDMs were cultured at $0.5–1 \times 10^6$ cells mL^{-1} in Dulbecco's modified Eagle's Medium (DMEM) supplemented with 1× penicillin/streptomycin (PS) and 10% fetal bovine serum (FBS) (Gibco). Primary BMDMs were cultured at $0.5–1 \times 10^6$ cells mL^{-1} in DMEM supplemented with 10% FBS, 10% macrophage colony-stimulating factor (M-CSF)-conditioned media, 1% HEPES, 1% sodium pyruvate, 1% glutamine. Cells were treated with doxycycline (Sigma), LPS from *Escherichia coli* 0111:B4 (Sigma) and ATP (Sigma).

ELISA: mIL-1β and mTNF-α assays were performed by using the DuoSet ELISA kits (R&D Systems).

Measurement of NLRP3-ATPase activity: Human recombinant NLRP3 (0.105 μg; BPS Bioscience, San Diego, CA, USA) was incubated with the assessed compounds in the reaction buffer (20 mM Tris-HCl, pH 7.8, 133 mM NaCl, 20 mM $MgCl_2$, 3 mM KCl, 0.56 mM EDTA, 0.5% DMSO) for 15 min at 37 °C. ATP (250 μM, Ultra Pure ATP) was added, and the mixtures were further incubated for 40 min at 37 °C. The hydrolysis of ATP by NLRP3 was determined by a luminescent ADP detection performed with ADP-Glo Kinase Assay (Promega, Madison, MI, USA) according to the manufacturer's protocol.

Computational methods

Docking simulations involved the NACHT domain of the human NLPR3 protein (residues 220–536, Entry Id: Q96P20, Entry Name: NLRP3_HUMAN), the homology model of which was generated by using the resolved structure of NLRC4 (PDB ID: 4KXF). Briefly, homology modeling was performed by Modeller 9.10 by using the default parameters;[36] among the 20 generated models, the best structure was selected according to the computed scores (i.e., DOPE and GA341) as well as to the percentage of residues falling in the allowed regions of the Ramachandran (91.2%) and chi plots (95.8%). The selected model was carefully checked to avoid unphysical occurrences such as *cis* peptide bonds, wrong configurations, improper bond lengths, nonplanar aromatic rings, or colliding side chains. To remain compatible with physiologic pH, Asp, Glu, Lys, and Arg residues were considered in their ionized forms, whereas His and Cys residues were maintained neutral by default. The so-completed model underwent a minimization procedure by

keeping the backbone atoms fixed to preserve the predicted folding, and the so-obtained final structure was used in the following docking simulations that involved ATP, taken as a reference ligand, plus the herein-reported inhibitors. The ATP structure was retrieved from the resolved structure (PDB ID: 4AFF), which showed the best resolution among those co-crystallized with ATP, and its conformation was optimized by the PM7 semiempirical method as implemented in MOPAC2012. In contrast, the conformational profile of the here-reported inhibitors was explored by Monte Carlo simulations, which generated 1000 minimized geometries by randomly rotating the rotatable bonds. The so-obtained lowest energy structure underwent the following docking simulations that were performed by using PLANTS and arranged in two steps.[40] The first step involved the docking of ATP; its search was focused on a 12 Å radius sphere around the highly conserved Lys232 residue, the key role of which was confirmed by previous studies. The so-computed complex was then minimized by keeping all atoms outside a 12 Å radius sphere fixed around the bound ATP, and the so-optimized NLPR3 structure was used in the docking analyses of the reported inhibitors by focusing the search on a 12 Å radius sphere around the bound ATP. In all docking simulations, 20 poses were generated and scored by using the ChemPLP score function with speed equal to 1. The computed best complexes for the proposed inhibitors were optimized with the same protocol already described for the ATP complex.

Acknowledgements

This work was supported by the Università degli Studi di Torino (Ric. Loc. 2014, Ric. Loc. 2015, and Ric. Loc. 2015 QUOTA B) and in part by the French National Research Agency (ANR-13-JSV3-0002-01 to B.P.) and the European Research Council (ERC-2013-CoG_616986 to B.P.). The authors thank Dr. Emad Alnemri (Thomas Jefferson University, USA) for sharing immortalized wild-type and NLRP3 KO murine bone-marrow-derived macrophages, Dr. Elisa Lupino (Università degli Studi di Torino) for kind assistance with the NLRP3 ATPase assay, and Dr. Marco Lucio Lolli (Università degli Studi di Torino) for access to the UHPLC instrument.

Keywords: acrylamide derivatives · drug design · inflammasomes · inflammation · pyroptosis

[1] G. Y. Chen, G. Nunez, *Nat. Rev. Immunol.* **2010**, *10*, 826 – 837.
[2] O. Takeuchi, S. Akira, *Cell* **2010**, *140*, 805 – 820.
[3] P. Pelegrin, A. Suprenant, *EMBO J.* **2006**, *25*, 5071 – 5082.
[4] S. Locovei, E. Scemes, F. Qui, D. Spray, G. Dahl, *FEBS Lett.* **2007**, *581*, 483 – 488.
[5] V. Compan, A. Baroja-Mazo, G. Lopez-Castejon, A. Gomez, C. M. Martinez, D. Angosto, M. T. Montero, A. S. Herranz, E. Bazan, D. Reimers, V. Mulero, P. Pelegrin, *Immunity* **2012**, *37*, 487 – 500.
[6] V. Compan, F. Martın-Sanchez, A. Baroja-Mazo, G. Lopez-Castejon, A. I. Gomez, A. Verkhratsky, D. Brough, P. Pelegrın, *J. Immunol.* **2015**, *194*, 1261 – 1273.
[7] P. Duewell, H. Kono, K. J. Rayner, C. M. Sirois, G. Vladimer, F. G. Bauernfeind, G. S. Abela, L. Franchi, G. Nunez, M. Schnurr, T. Espevik, E. Lien, K. Fitzgerald, A. Rock, K. J. Moore, S. D. Wright, V. Hornung, E. Latz, *Nature* **2010**, *464*, 1357 – 1361.
[8] F. Martinon, V. Petrilli, A. Mayor, A. Tardivel, J. Tschopp, *Nature* **2006**, *440*, 237 – 241.
[9] A. Halle, V. Hornung, G. C. Petzold, C. R. Stewart, B. G. Monks, T. Reinheckel, K. A. Fitzgerald, E. Latz, K. J. Moore, D. T. Golenbock, *Nat. Immunol.* **2008**, *9*, 857 – 865.
[10] M. Lamkanfi, V. M. Dixit, *Cell* **2014**, *157*, 1013 – 1022.
[11] F. S. Sutterwala, S. Haasken, S. L. Cassel, *Ann. N. Y. Acad. Sci.* **2014**, *1319*, 82 – 95.
[12] H. Guo, J. B. Callaway, J. P-Y. Tang, *Nat. Med.* **2015**, *21*, 677 – 687.
[13] L. Agostini, K. Burns, M. F. McDermott, P. N. Hawkins, J. Tschopp, *Immunity* **2004**, *20*, 319 – 325.
[14] R. Goldbach-Mansky, N. J. Dailey, S. W. Canna, A. Gelabert, J. Jones, B. I. Rubin, H. J. Kim, C. Brewer, C. Zalewski, E. Wiggs, S. Hill, M. L. Turner, B. I. Karp, I. Aksentijevich, F. Pucino, S. R. Penzak, M. H. Haverkamp, L. Stein, B. Adams, T. L. Moore, R. C. Fuhlbrigge, B. Shaham, J. N. Jarvis, K. O'Neil, R. K. Vehe, L. O. Beitz, G. Gardner, W. P. Hannan, R. W. Warren, W. Horn, J. L. Cole, S. M. Paul, P. N. Hawkins, T. H. Pham, C. Snyder, R. A. Wesley, S. C. Hoffmann, S. M. Holland, J. A. Butman, D. L. Kastner, *N. Engl. J. Med.* **2006**, *355*, 581 – 592.
[15] M. Gattorno, S. Tassi, S. Carta, L. Delfino, F. Ferlito, M. A. Pelagatti, A. D'Osualdo, A. Buoncompagni, M. G. Alpigiani, M. Alessio, A. Martini, A. Rubartelli, *Arthritis Rheum.* **2007**, *56*, 3138 – 3148.
[16] A. Baroja-Mazo, F. Martín-Sánchez, A. I. Gomez, C. M. Martínez, J. Amores-Iniesta, V. Compan, M. Barberà-Cremades, J. Yagüe, E. Ruiz-Ortiz, J. Antón, S. Buján, I. Couillin, D. Brough, J. I. Arostegui, P. Pelegrín, *Nat. Immunol.* **2014**, *15*, 738 – 750.
[17] H. M. Lee, J. J. Kim, H. J. Kim, M. Shong, B. J. Ku, E. K. Jo, *Diabetes* **2013**, *62*, 194 – 204.
[18] M. T. Heneka, M. P. Kummer, A. Stutz, A. Delekate, S. Schwartz, A. Vieira-Saecker, A. Griep, D. Axt, A. Remus, T. C. Tzeng, E. Gelpi, A. Halle, M. Korte, E. Latz, D. T. Golenbock, *Nature* **2012**, *493*, 674 – 678.
[19] A. G. Baldwin, D. Brough, S. Freeman, *J. Med. Chem.* **2016**, 59, 1691 – 1710.
[20] J. A. MacDonald, C. P. Wijekoon, K. C. Liao, D. A. Muruve, *IUBMB Life* **2013**, *65*, 851 – 862.
[21] J. A. Duncan, D. T. Bergstralh, Y. Wang, S. B. Willingham, Z. Ye, A. G. Zimmermann, J. P. Ting, *Procl. Natl. Acad. Sci. USA* **2007**, *104*, 8041 – 8046.
[22] M. Cocco, D. Garella, A. Di Stilo, E. Borretto, L. Stevanato, M. Giorgis, E. Marini, R. Fantozzi, G. Miglio, M. Bertinaria, *J. Med. Chem.* **2014**, *57*, 10366 – 10382.
[23] R. A. Bauer, *Drug Discovery Today* **2015**, *20*, 1061 – 1073.
[24] C. Marchetti, J. Chojnacki, S. Toldo, E. Mezzaroma, N. Tranchida, S. W. Rose, M. Federici, B. W. Van Tassell, S. Zhang, A. Abbate, *J. Cardiovasc. Pharmacol.* **2014**, *63*, 316 – 322.
[25] M. Lamkanfi, J. L. Mueller, A. C. Vitari, S. Misaghi, A. Fedorova, A. K. Deshayes, W. P. Lee, H. M. Hoffman, V. M. Dixit, *J. Cell Biol.* **2009**, *187*, 61 – 70.
[26] M. C. Noe, A. M. Gilbert, *Annu. Rep. Med. Chem.* **2012**, *47*, 413 – 439.
[27] J. Uetrecht, *Chem. Res. Toxicol.* **2009**, *22*, 24 – 34.
[28] X. Zhang, F. Liu, X. Chen, X. Zhu, J. Uetrecht, *Drug Metab. Pharmacokinet.* **2011**, *26*, 47 – 59.
[29] M. E. Flanagan, J. A. Abramite, D. P. Anderson, A. Aulabaugh, U. P. Dahal, A. M. Gilbert, C. Li, J. Montgomery, S. R. Oppenheimer, T. Ryder, B. P. Schuff, D. P. Uccello, G. S. Walker, Y. Wu, M. F. Brown, J. M. Chen, M. M. Hayward, M. C. Noe, R. S. Obach, L. Philippe, V. Shanmugasundaram, M. J. Shapiro, J. Starr, J. Stroh, Y. Che, *J. Med. Chem.* **2014**, *57*, 10072 – 10079.
[30] L. Regazzoni, L. Del Vecchio, A. Altomare, K. J. Yeum, D. Cusi, F. Locatelli, M. Carini, G. Aldini, *Free Radical Res.* **2013**, *47*, 172 – 180.
[31] H. M. Hoffman, J. L. Mueller, D. H. Broide, A. A. Wanderer, R. D. Kolodner, *Nat. Genet.* **2001**, *29*, 301 – 305.
[32] H. M. Hoffman, S. G. Gregory, J. L. Mueller, M. Tresierras, D. H. Broide, A. A. Wanderer, R. D. Kolodner, *Hum. Genet.* **2003**, *112*, 209 – 216.
[33] C. Dodé, N. Le Du, L. Cuisset, F. Letourneur, J-M. Berthelot, G. Vaudour, A. Meyrier, R. A. Watts, D. G. I. Scott, A. Nicholls, B. Granel, C. Frances, F. Garcier, P. Edery, S. Boulinguez, J.-P. Domergues, M. Delpech, G. Grateau, *Am. J. Hum. Genet.* **2002**, *70*, 1498 – 1506.
[34] S. D. Brydges, J. L. Muller, M. D. McGeough, C. A. Pena, A. Misaghi, C. Gandhi, C. D. Putnam, D. L. Boyle, G. S. Firestein, A. A. Horner, P. Soroosh, W. T. Watford, J. J. O'Shea, D. L. Kastner, H. M. Hoffman, *Immunity* **2009**, *30*, 875 – 887.
[35] G. Meng, F. Zhang, I. Fuss, A. Kitani, W. Strober, *Immunity* **2009**, *30*, 860 – 874.

[36] M. A. Martí-Renom, A. Stuart, A. Fiser, R. Sánchez, F. Melo, A. Sali, *Annu. Rev. Biophys. Biomol. Struct.* **2000**, *29*, 291 – 325.
[37] G. Aldini, G. Vistoli, L. Regazzoni, L. Gamberoni, R. M. Facino, S. Yamaguchi, K. Uchida, M. Carini, *Chem. Res. Toxicol.* **2008**, *21*, 824 – 835.
[38] Y. Hashizume, M. Hirota, H. Koike, Y. Matsumoto, S. Mihara, H. Nakamura (Pfizer Japan, Inc.), Int. PCT Pub. No. WO2006134485 A1, **2006**.
[39] Z. Zhang, A. G. Marshall, *J. Am. Soc. Mass Spectrom.* **1998**, *9*, 225 – 233.
[40] O. Korb, T. Stützle, T. E. Exner, *J. Chem. Inf. Model.* **2009**, *49*, 84 – 96.

Received: January 28, 2016
Published online on ■■ ■■, 0000

CAPS block is on! Cryopyrin-associated periodic syndromes (CAPS) are rare genetic diseases caused by gain-of-function mutations in NLRP3. Overactivation of the NLRP3 inflammasome is also involved in other metabolic diseases. Herein, a series of acrylamides that inhibit NLRP3-dependent pyroptosis and IL-1β release from CAPS-mutant macrophages are reported. Direct inhibition of NLRP3 ATPase in human isolated NLRP3 has emerged as a potential target for this compound class.

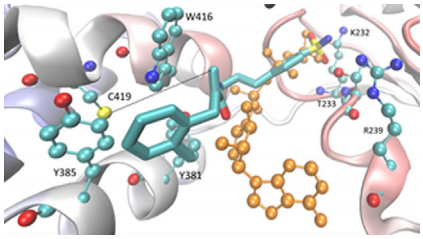

*M. Cocco, G. Miglio, M. Giorgis, D. Garella, E. Marini, A. Costale, L. Regazzoni, G. Vistoli, M. Orioli, R. Massulaha-Ahmed, I. Détraz-Durieux, M. Groslambert, B. F. Py, M. Bertinaria**

■■ – ■■

Design, Synthesis, and Evaluation of Acrylamide Derivatives as Direct NLRP3 Inflammasome Inhibitors

These are not the final page numbers! ↗↗